Structure and ionic diffusivity in an yttria-stabilised zirconia/strontium titanate multilayer

Wei Li Cheah[a,1], David W. McComb[b], Michael W. Finnis[a,c,*]

[a] *Department of Materials, Imperial College London, Royal School of Mines, Exhibition Road, London SW7 2AZ, UK*
[b] *Department of Materials Science and Engineering, The Ohio State University, Columbus, Ohio 43210, United States*
[c] *Department of Physics, South Kensington Campus, Imperial College London, London SW7 2AZ, UK*

Abstract

Enhanced ionic conductivity observed in a heteroepitaxial multilayer of yttria-stabilised zirconia and (YSZ) and strontium titanate (STO) has variously been attributed to lattice dilation or a disordered oxygen sublattice, leading to high interfacial mobility of anions, as compared to those of the constituent bulk oxides. We seek to understand the mechanism of ionic motion in such heterostructures by first simulating the atomic structure assuming coherent interfaces. After investigating possible low-energy interface structures using a genetic algorithm, we perform molecular dynamics simulations on these structures to examine the anionic diffusivity in the system. We find that the extreme biaxial tensile strain in the YSZ layer, as imposed between layers of STO, induces phases that differ from fluorite. The lowest energy structure is an unknown phase, which we refer to as quasi-cubic and whose cation sublattice resembles an extension of the perovskite; this structure does not lead to enhanced ionic conductivity.

Keywords: Interface, Atomic structure, Strain accommodation, Ionic diffusion, Atomistic simulation

1. Introduction

Pure ZrO_2, at ambient temperature and pressure, exists in the monoclinic (baddeleyite) phase, transforming to the tetragonal phase at 1440 K and then the cubic fluorite phase at 2640 K [1]. The formation of the latter phases are not restricted to high temperatures only, for these phases may be stabilised at lower temperatures by oxygen vacancies introduced into the lattice with aliovalent doping [2]. The vacancies, which compensate for the charge difference between the Zr^{4+} host ions and the aliovalent substituent ions, play another perhaps more important role in that they provide low energy paths for oxygen ion migration through the lattice via vacancy hopping. Yttria-stabilised zirconia (YSZ) is one such oxygen ion conductor, whose oxygen ion mobility at elevated temperatures is sufficiently high for industrial applications such as an electrolyte in high temperature solid oxide fuel cells (SOFC) [3, 4].

However, its ionic conductivity at lower temperatures leaves much to be desired[5]. A popular approach to address this limitation in recent years has been to manipulate the dimensions of the lattice

*Corresponding author
Email address: m.finnis@imperial.ac.uk (Michael W. Finnis)
[1] Present address: Institute of High Performance Computing, 1 Fusionopolis Way, #16-16 Connexis North, Singapore 138632

of the material such that the energy barrier for vacancy hopping is reduced [6, 7]. This effect has been demonstrated only theoretically at extreme compression of the lattice[8], but has been realized experimentally for lattices under expansive strain. By growing very thin oxide films epitaxially on carefully selected single crystal substrates, so that the interface is coherent or semi-coherent, the oxide lattice can be forced to alter its dimensions to accommodate the underlying lattice of the substrate material. For YSZ films deposited onto substrates such as Lu_2O_3, Y_2O_3, MgO and $Gd_2Zr_2O_7$, which imposes modest biaxial tensile strains of up to 3% on the YSZ lattice, the ionic conductivity of the film increases by up to two orders of magnitude in comparison with the same material in the bulk [9, 10, 11]. Replacing the substrate material with (001) $SrTiO_3$ (STO) would result in a tensile strain of 7% in the (001) YSZ lattice, supposing a perfectly coherent interface between the substrate and the film; such a heterostructure of a 1 nm-thick YSZ layer sandwiched between layers of STO reportedly achieves eight orders of magnitude enhancement in conductivity, which, it was suggested, is due to greatly increased ionic mobility at the highly strained interfacial planes [12].

If the main contribution to the measured conductivity is indeed ionic, such a dramatic improvement is unprecedented. Electronic conductivity is more likely to attain this magnitude, and could arise from unintentional p-type doping of the STO substrate [13, 14, 15, 16]. The fact that the YSZ/STO interface is observed to be atomically sharp and completely coherent is equally unexpected, as the enormous amount of strain is more likely to have been relieved by dislocations which may possibly contribute to enhanced ionic conductivity [17]. An attempt to reproduce the result [18] revealed that the orientation and growth mode of the deposited YSZ film depends on the termination plane of the (001) STO substrate. When a SrO plane terminates the substrate, the YSZ film grows epitaxially with (001) orientation, whereas a TiO_2-terminated substrate result in island growth of tilted (111) YSZ. Another study [19] finds a dependence of the YSZ film orientation on the growth rate: slow deposition rates yield highly coherent (001) films on TiO_2-terminated STO but higher deposition rates at the same growth temperature produce incoherent islands of (110) YSZ that are partially connected. The conductivity of the film is then found to correlate with the epitaxial quality of the film, with the former having high conductivity but that of the latter comparable to a bare STO substrate. In contrast, a YSZ/STO multilayer, fabricated using a different method in another investigation [20], exhibits enhanced conductivity of similar magnitude to that of the coherent STO/$YSZ_{(1nm)}$/STO trilayer[12], although in this case the YSZ layer is discontinuous and formed of YSZ islands with both (001) and (110) orientations. Nonetheless, the increased conductivity in this specimen appears not to be ionic, as the authors observed no diffusion of isotopes in their ^{18}O tracer experiments.

While reports on the conductivity measurements of the YSZ/STO system have been contradictory, there have been several theoretical studies seeking to understand the origin of the observed enhancement. As tensile strain of the lattice has been shown to result in an increase in ionic conductivity, these

theoretical works examine whether extreme expansion of bulk YSZ lattice could produce massively enhanced ionic mobility. In almost all of these works, the YSZ lattice is assumed to be fluorite. Several investigations on anionic diffusivity in ZrO_2 as a function of biaxial strain revealed an optimum strain at 3% and 4% using classical and density functional theory (DFT) calculations respectively, with an improvement in the diffusivity of at most four orders of magnitude [21, 22, 23]. While these results are unable to explain the high conductivity observed experimentally, the authors of these papers, as well as those of several other works, make an interesting observation. Above the optimum strain, local geometry optimisation of the strained fluorite lattice produces a structural transformation. In two of these works, the authors note a change in coordination of the ions [21, 22]. In references 23, 24, 25, 26, the authors show their resulting structures in which the coordination of the Zr^{4+} ion with the O^{2-} ions is sixfold instead of eightfold as in the fluorite phase, strongly resembling the columbite (α-PbO_2) phase. In agreement with these results, a study on the stability of various theoretical structures of ZrO_2 with strain, finds several phases more stable than the fluorite phase at high values of strain, most of which consist of Zr^{4+} ions in sixfold coordination. One of the most stable of these is the columbite phase [27].

Pennycook *et al.* find, using simulated annealing with DFT, yet another phase of ZrO_2 that transforms from 7%-strained cubic fluorite lattice [28]. They describe the oxygen sublattice as being arranged in a 'zigzag' manner when the lattice is projected onto the (001) plane . When YSZ is layered with STO, they find a disordered oxygen sublattice from their simulations and also observe this from elemental maps of oxygen with electron energy loss spectroscopy (EELS) [29]. Performing *ab initio* molecular dynamics (MD) simulations on bulk pure ZrO_2 with the zigzagged oxygen sublattice, they calculate six orders of magnitude enhancement in the ionic conductivity of this structure relative to that of the unstrained stabilised fluorite phase in the bulk.

Clearly, the straining of the ZrO_2 lattice by itself is not able to simulate eight orders of magnitude enhancement in the ionic conductivity of the YSZ/STO system, even when accompanied by a change in the structure. However, the effect of STO when layered with YSZ, on the diffusivity of oxygen ions in the multilayer has not been reported and so the mechanism for ionic diffusion in the system has not yet been examined. We therefore present in this report our investigation of coherent YSZ/STO structures and calculations of oxygen ion diffusivities in the system. As the strained bulk ZrO_2 studies mentioned above suggest strongly the need to consider phase changes in highly strained states, we probe the phase space using a hybrid strategy to seek low energy structures. Classical interatomic potentials, being cheap to compute, are first used in conjunction with a genetic algorithm to obtain a set of plausible structures. Since these potentials are limited in predicting energies with quantitative as well as qualitative accuracy, we then perform DFT calculations to further relax the geometries in order to obtain a more reliable ordering and magnitude of the energies. We find a stable YSZ phase with both SrO and TiO_2-terminated STO layers, whose cation sublattice resembles those of perovskite as well as

fluorite but whose oxygen ion sublattice is different from those of oxides that we are aware of. This phase is further stabilised by intermixing between the YSZ and STO layers. MD simulations that we perform on these multilayer structures suggest a mechanism for oxygen ion diffusion within the YSZ layers, but our calculated diffusivities and activation energies of the oxygen ions indicate no enhancement of ionic conductivities, but rather a reduction in the oxygen ion mobility as compared to that in bulk YSZ.

2. Computational details

We construct three configurations of YSZ/STO multilayers in periodic supercells with interfacial areas that are equivalent to 2×2 unit cells of STO. When we make the STO layer 2.5 unit cells thick, the termination planes on either side of the layer are both SrO planes or TiO_2 planes; we consider these two cases and refer to these supercells as having SrO interfaces and TiO_2 interfaces respectively. In the third supercell with interfaces that we label as "mixed interfaces", the STO layer is 2 unit cells thick and thus is terminated with a SrO plane on one side and a TiO_2 plane on the other. In each of our supercells we strain 1.5 unit cells thick of fluorite ZrO_2 layer on the STO layer in the orientation suggested by Garcia-Barriocanal *et al.*: the [001] direction of the fluorite lattice is parallel to the [001] direction of the perovskite lattice but rotated 45° about [001], i.e. $[110](001)_{\mathrm{YSZ}} \parallel [100](001)_{\mathrm{STO}}$ [12]. To introduce 8 mol% of Y_2O_3 doping in the ZrO_2 layer, two Y^{3+} ions replace two randomly selected Zr^{4+} ions, with one also randomly selected O^{2-} ion removed to maintain the overall charge neutrality of the supercell.

2.1. Identifying stable and metastable structures

To explore the phase space of the YSZ/STO multilayer structure we use a genetic algorithm, an optimisation method that is capable of evolving an interface structure to the one with the global minimum energy. In many optimisation techniques including simulated annealing and the present genetic algorithm, sometimes referred to as 'global optimisation' methods, metastable structures are found, where the system becomes trapped, sometimes for a long time, in a local minimum of the energy landscape. This can be advantageous; we find it useful to generate a collection of the longer-lived or more frequently recurring, low energy metastable structures in addition to the lowest energy structure. The genetic algorithm that we apply in our search [30] has been previously demonstrated in simulations of bulk and grain boundaries of STO, bulk ZrO_2 and pure ZrO_2/STO multilayers [30, 27].

Assigning random coordinates to the ions at each YSZ interfacial plane, but confining them to within the interfacial region, we use such configurations as the initial configurations for our genetic algorithm simulations with the same genetic algorithm parameters as given in reference 30. Five separate genetic algorithm runs were made for each type of YSZ/STO configuration, with each run reaching at least 5000 generations, which is sufficient to identify low energy structures including metastable configurations.

We evaluate the energies of the structures using Buckingham potentials for short-ranged interactions and a Coulombic term for longer-range interactions. These potentials are cheap to compute, whereas

Table 1: The parameters for the Buckingham potentials of STO and YSZ, taken from references 32* and 33†

Interactions	A(eV)	ρ(Å)	C(eVÅ^6)
Sr-O*	682.172	0.39450	0
Ti-O*	2179.122	0.30384	8.986
O-O†	9547.960	0.21916	32.000
Y-O†	1766.400	0.33849	19.430
Zr-O†	1502.110	0.34770	5.100

using DFT with the genetic algorithm would be prohibitively expensive. Treating the ions as rigid bodies with fixed formal charges, the pairwise potential $V(r_{ij})$ acting between atoms i and j is expressed below:

$$V(r_{ij}) = A\exp\left(\frac{-r_{ij}}{\rho}\right) - \frac{C}{r_{ij}^6} + \frac{q_i q_j}{r_{ij}}$$

where q_i and q_j are the fixed formal charges of atoms i and j respectively, and r_{ij} is the distance between the two atoms. The parameters A, ρ and C for STO and YSZ are listed in Table 1; the reliability and transferability of these potentials for bulk STO and ZrO_2 are discussed and compared elsewhere [31, 27]. Results of calculations using these potentials have also been shown to have reasonable qualitative agreement with DFT-based computations in the relative energetic ordering of strained pure ZrO_2 structures [27].

Nonetheless we select several low energy structures from our genetic algorithm simulations and validate the energies of our structures with those calculated using the more accurate DFT approach. The DFT computations are performed within the local density approximation (LDA) implemented in the plane wave-based electronic structure code CASTEP [34]. Our calculations employ ultrasoft pseudopotentials for the elements generated within CASTEP, treating the semicore states of Sr, Ti , Y and Zr explicitly, with an energy cut-off of 600 eV and a Monkhurst-Pack mesh of $4 \times 4 \times 2$ k-points. We constrain the supercells laterally to the theoretical lattice dimensions of STO (calculated to be 3.856 Å using this method) while optimising the atomic positions, c lattice parameter and angles α, β using the Broyden-Fletcher-Goldfarb-Shanno (BFGS) method [35, 36, 37, 38]. For this geometry relaxation, the ionic forces are converged to 0.05 eVÅ^{-1}.

To compare the energies between the interface structures, we evaluate the interfacial energies in the same way as in reference 27. In general the interfacial energy γ has the form:

$$\gamma = (G - \sum_i \mu_i N_i)/A. \quad (1)$$

We encompass both the interfaces within our supercell in this definition, in which G is the Gibbs free energy of the total supercell and N_i is the number of molecules of component i in the supercell, which has cross-sectional area A. The components, which are labelled i, have chemical potentials μ_i. We choose to define the components of our system from the set ZrO_2, Y_2O_3, SrO, TiO_2 and $SrTiO_3$, where in

equilibrium we would have $SrTiO_3 = SrO + TiO_2$.

The treatment of the two closely spaced interfaces as a single interface for the purpose of calculating the excess interfacial energy is physically motivated, because the separation into two interfacial energies would be unphysical unless the two interfaces are separated by some homogeneous phase of sufficient thickness to isolate one from the influence of the other. In practice we always evaluate the zero-temperature internal energy as an approximation to the Gibbs energy.

Comparing the interfacial energies of configurations with the same stoichiometry but with different interface structures, the chemical potential terms cancel and we have the following expression:

$$\gamma_{\mathrm{S}}^{\mathrm{int}} - \gamma_{\mathrm{ref}}^{\mathrm{int}} = \frac{G_{\mathrm{S}}^{\mathrm{int}} - G_{\mathrm{ref}}^{\mathrm{int}}}{A} \tag{2}$$

Superscript "int" refers to the stoichiometry of the $SrTiO_3$ termination, while subscript "S" and "ref" refer to the structure being evaluated and the reference structure respectively. For configurations with similar interface structures but having different stoichiometries, only the terms with μ_{ZrO_2} and $\mu_{Y_2O_3}$ cancel because each has the same N_{ZrO_2} and $N_{Y_2O_3}$. Thus from Equation 1 and defining $\gamma_{\mathrm{S}}^{\mathrm{a}}$ and $\gamma_{\mathrm{S}}^{\mathrm{b}}$ as the interfacial energies of structure S at the SrO-rich and TiO_2-rich limits respectively, we derive an expression for the difference between these two interfacial energies [27]:

$$\gamma_{\mathrm{S}}^{\mathrm{a}} - \gamma_{\mathrm{S}}^{\mathrm{b}} = \frac{\Delta G_{\mathrm{f,STO}}^{0}(N_{TiO_2} - N_{SrO})}{A} \tag{3}$$

where the standard free energy of formation of $SrTiO_3$, $\Delta G_{\mathrm{f,STO}}^{0} = \mu_{\mathrm{STO}} - \mu_{TiO_2}^{0} - \mu_{SrO}^{0}$. $\mu_{TiO_2}^{0}$ and μ_{SrO}^{0} are the chemical potentials of TiO_2 and SrO at standard temperature and pressure respectively.

2.2. Seeking low barrier paths for oxygen diffusion

Selecting two especially low energy configurations, we investigate oxygen ion diffusion in these structures by performing classical-based MD simulations with the Buckingham potentials described above, at constant pressure and temperature (NPT ensemble) using the leapfrog verlet algorithm with the Nose-Hoover and Melchionna thermostat and barostat as implemented in the General Utility Lattice Programme (GULP) [39]. With our supercells scaled by 3×3 parallel to the interfacial plane and a timestep of 1.0 fs, we allow the systems to equilibrate for 60 ps before running the simulations for 2000 ps at temperatures between 800 to 2750 K. Although our two selected configurations are in fact metastable in the classical description of the interatomic potentials, they do not undergo any phase transformation below 2750 K within our simulated MD time.

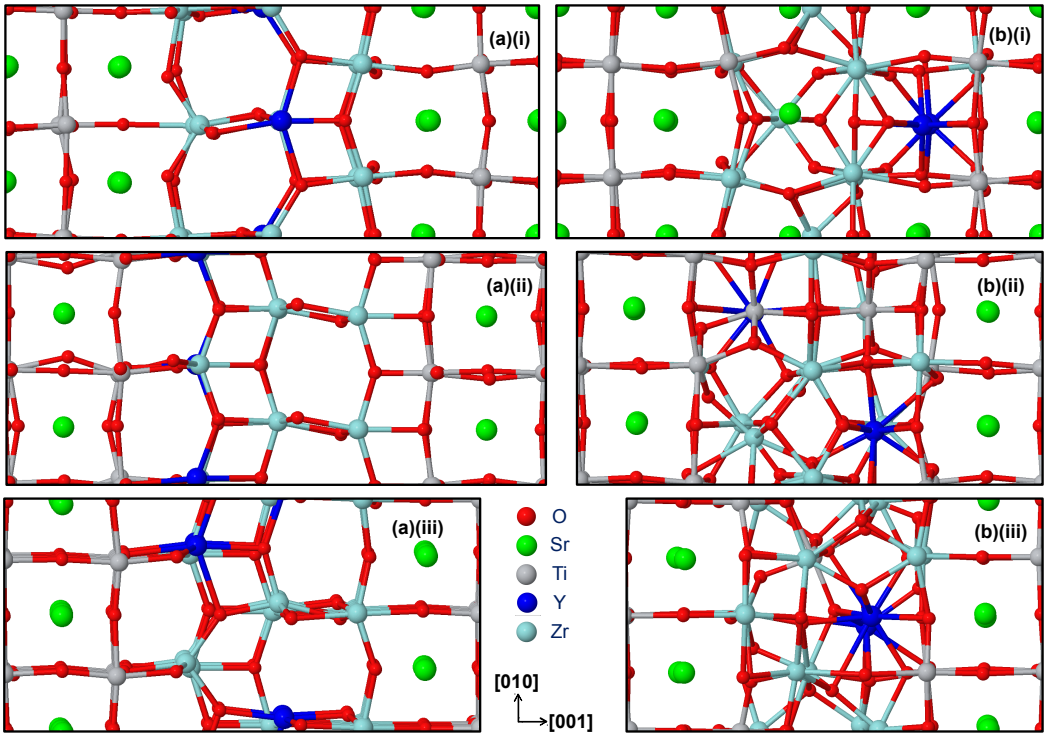


Figure 1: The lowest energy structures of (a) anatase-like and (b) quasi-cubic structures in epitaxy with (i) SrO- (ii) TiO_2- and (iii) 'mixed' interfaces.

.

3. Results and Discussions

For all three STO stoichiometries that we have considered, our genetic algorithm simulations of the YSZ/STO configurations find the initial configurations with the YSZ layers in the fluorite phase to be unstable. The most stable phase that we observe in all three cases is an anatase-like YSZ phase in perfectly coherent epitaxy with the STO layer, consistent with the finding in another work of the greater stability of a pure ZrO_2 layer in an anatase-like phase compared to a highly strained fluorite layer when the ZrO_2 layer forms a coherent interface with the STO layer [27]. Figures 1(a)(i-iii) illustrate these configurations.

We also identify an additional structure that appears in our simulations as a long-lived transient and is quite unlike the anatase or even the higher energy rutile, columbite, or pyrite structures reported for pure ZrO_2 layers in ZrO_2/STO systems [27]. For ease of reference, we will refer to this unknown phase as the 'quasi-cubic' phase. We show configurations with quasi-cubic YSZ layers for each type of interface in Figure 1(b)(i-iii).

To our knowledge, the YSZ lattices in Figures 1(b) do not resemble any structures of established ionic compounds. The O^{2-} sublattices of the YSZ layers in all three configurations bear little resemblance to that of bulk fluorite, though the cation sublattices coincide with that of a fluorite structure in Garcia-Barriocanal's postulated orientation of 45° rotated about the [001] axis [12]. In this orientation, we note

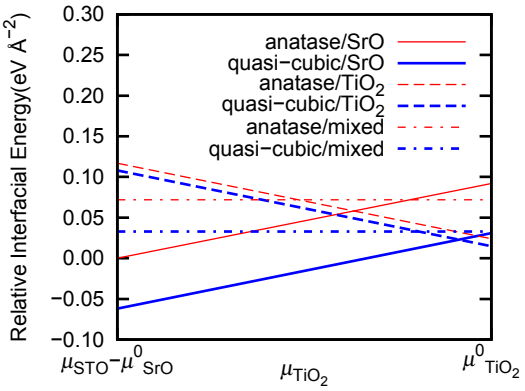


Figure 2: Variation of relative interfacial energies of anatase–like and quasi–cubic YSZ/STO epitaxial structures with SrO, TiO_2 and mixed interfaces over a range of μ_{TiO_2}. On the left of the x-axis, STO is in equilibrium with SrO ($\mu_{TiO_2} = \mu_{STO} - \mu^0_{SrO}$); on the right, with TiO_2($\mu_{TiO_2} = \mu^0_{TiO_2}$).

that the face-centred cubic fluorite lattice could be redefined as a body-centred tetragonal whose cation lattice is topologically similar to that of a body-centred tetragonal perovskite (hence the label 'quasi-cubic'). The YSZ/STO configurations additionally exhibit mixing between the two layers. Thus the structures may also be thought of as a defective (Sr,Y)(Ti,Zr)O_3 perovskite structure with an unusual O^{2-} sublattice in the region where there are some Zr^{4+} or Ti^{4+} ions in the A-site of a perovskite ABO_3 lattice. The anion sublattice is reminiscent of the disordered sublattice structure that have been reported for a YSZ/STO epitaxial structure [28, 40].

Because of the intermixing between the layers, as well as the two interfaces in each configuration being inequivalent, it is impossible for us to extract a unit cell of the quasi-cubic phase from the multilayer configuration. We are therefore unable to calculate its energy in the bulk phase for comparison with other known and hypothetical ZrO_2 polymorphs, and so unable to determine whether the existence of the quasi-cubic phase is a strain or interface effect. We can, however compare the energies of the configurations in the multilayer form. With the energies evaluated with the classical potentials, these quasi-cubic structures with SrO, TiO_2, and mixed interfaces are only metastable, with interfacial energies 0.006 eV Å^{-2}, 0.115 eV Å^{-2} and 0.126 eV Å^{-2} higher than their anatase-like counterparts respectively. To compute the energies with higher accuracy, we relaxed the coordinates within DFT. We find that the quasi-cubic structures are in fact more stable than the anatase-like ones by 0.062 eV Å^{-2}, 0.009 eV Å^{-2} and 0.039 eV Å^{-2} respectively. Between these quasi-cubic configurations, we find that the one with SrO interfaces is the most stable structure across most of the range of possible μ_{TiO_2}, as shown in Figure 2 which plots the relative energies of the interfaces as a function of the chemical potential of TiO_2, with the anatase-like system having SrO interfaces in the SrO-rich limit as the reference point. The quasi-cubic structure with TiO_2 interfaces is predicted to be stable only at high μ_{TiO_2}.

Thus we choose the quasi-cubic structure with SrO interfaces as one of particular interest and investi-

gate the atomic structure in detail in the following sections, so that we can relate calculated diffusivities of the O^{2-} ions to the atomic structure. We also examine the structure of the quasi-cubic configuration with TiO_2 interfaces and its O^{2-} ion diffusivity, since Garcia-Barriocanal *et al.* [12] suggested that the YSZ layer grows on TiO_2-terminated STO.

3.1. The quasi-cubic YSZ/STO structure with SrO interfaces

The intermixing of the layers in the quasi-cubic structure with SrO interfaces make a unique identification of the interface planes impossible. Nevertheless for the purpose of discussion it is convenient to consider the final structure as consisting of a YSZ layer and a STO layer. Two possible assignments of these layers present themselves. The region with the most ZrO_2 molecules might be assigned as the YSZ layer, as indicated in Figure 3, where the layer is originally intended to be from the initial configuration. Assigning the YSZ region in this way would mean that all of the Y^{3+} ions have diffused to the SrO termination plane of the STO layer and that the YSZ layer is approximately 0.6 nm thick. Alternatively, the diffused Y^{3+} ions might be included in the assignment of the YSZ layer as indicated in Figure 4, giving an apparent layer thickness of about 0.8 nm. For the purpose of investigating the intermixing of the layers, the former assignment is the more logical choice; thus we use the former.

In this configuration, the two Y^{3+} ions are in Sr^{2+} lattice sites and a Zr^{4+} ion is in a Ti^{4+} site, and vice versa. The arrangement of the diffused Y^{3+} cations is such that the Y^{3+} ions lie exclusively in rows in the [100] direction alternating with [100] rows of Sr^{2+} ions, as can be observed in Figure 1(b)(i). Within the YSZ layer, the diffused Sr^{2+} ions are ordered in [110] directions, in alternating rows with Zr^{4+} ions. We find that such intermixing is energetically favourable; to phase-separate this configuration requires an energy of 0.860 eV per supercell, calculated with DFT.

The local coordination of the cations is generally a useful characteristic of a bulk structure which we now consider in relation to the interface structures that have emerged. Cation coordination is usually explained by 'radius ratio' rules [41]. Thus the bulk structures of TiO_2 involve Ti^{4+} ions that are sixfold-coordinated by O^{2-} ions, as in the rutile or anatase structure. On the other hand, the larger Zr^{4+} ion in ZrO_2 adopts eightfold coordination in the high-temperature fluorite structure of pure ZrO_2, but this cation is not quite large enough to stabilise the fluorite at lower temperatures, nor are they small enough to stabilise the sixfold-coordinated structures. Thus the room temperature structure of ZrO_2 which is monoclinic, is sevenfold-coordinated, having a mixture of sixfold rutile-like and eightfold fluorite-like bonding.

In the case of the quasi-cubic structures, the Zr^{4+} ions are in coordinations ranging from sixfold to eightfold as indicated in Figure 3. At the interfacial plane of the YSZ layer consisting of $(ZrO_2)_3TiO_2$, the Zr^{4+} ions are in sixfold coordination, similar to the Ti^{4+} ions in perovskite $SrTiO_3$; this atomic plane appears to be a distorted version of the TiO_2 plane in STO. The Zr^{4+} ion occupying a Ti^{4+} lattice site within the STO layer is also sixfold coordinated. The rest of the Zr^{4+} ions within the YSZ layer

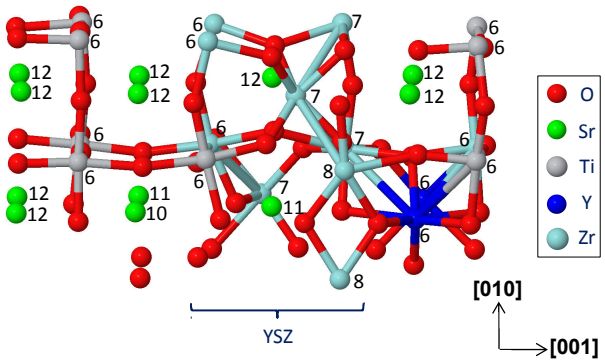


Figure 3: The coordination numbers of the cations with O^{2-} ions in the quasi-cubic epitaxial structure with SrO interfaces. The YSZ layer in this instance is defined as shown.

are sevenfold and eightfold coordinated with O^{2-} ions. The Ti^{4+} and Sr^{2+} ions are in the expected sixfold and twelvefold coordinations respectively as in bulk STO, with a few exceptions. One of the Sr^{2+} ions within the YSZ layer is elevenfold coordinated while a couple at the SrO interfacial plane are in tenfold and elevenfold coordination. The Y^{3+} ions, although occupying Sr^{2+} lattice sites, are not twelvefold-coordinated with the anions. Having a smaller ionic radius than a Sr^{2+} ion, only six O^{2-} ions can be found within the first neighbour shell of each Y^{3+} ion. Thus from the perspective of the local coordinations of the cations in this configuration, while the STO layer maintains its perovskite structure, the variety of environment of the cations in the YSZ layer further complicated by the intermixing between the layers makes it impossible to make a simple characterization of its structure.

3.2. Oxygen vacancy and diffusion in the quasi-cubic YSZ/STO structure with SrO interfaces

Oxygen diffusion is widely thought to occur by a vacancy hopping mechanism. However, this description requires the vacancies to be localised on a lattice. For the present interfaces, we have attempted to discover the location of our oxygen vacancy by mapping the electron density, which in bulk crystal would reveal a compact region of low density within a single vacant site. From the electron density map of the structure illustrated in Figure 4(a), the vacancy is clearly not localised; instead, there are several small low density regions distributed within the YSZ layer. The diffusion mechanism therefore must differ from the expected vacancy hopping.

To examine the ionic conduction mechanism that may be present in the structure, we perform MD simulations and trace the paths of diffusing O^{2-} ions. Using the same interatomic potentials as before, the metastable quasi-cubic YSZ layer might be expected to transform to the more stable anatase phase during the simulations. For simulations with temperatures of up to 2600 K, we detect no trace of phase evolution over the 10 ns simulation time, with negligible cation mean squared displacements (MSD); transformation from the quasi-cubic structure to the anatase one would have involved significant rearrangement of the cations. As we find that the O^{2-} ions within the STO layer merely vibrate about their equilibrium positions, we exclude the MSD contribution of these ions from our analysis and redefine

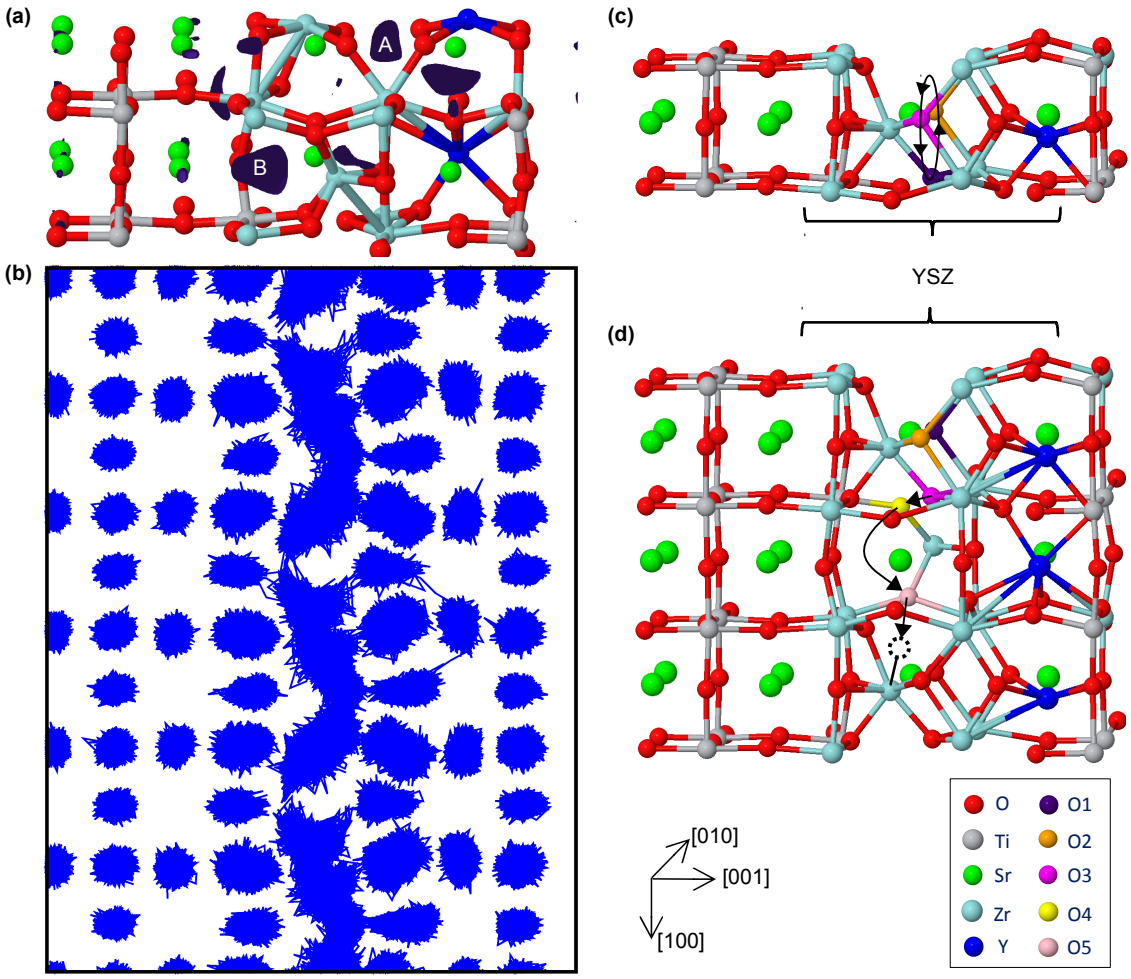
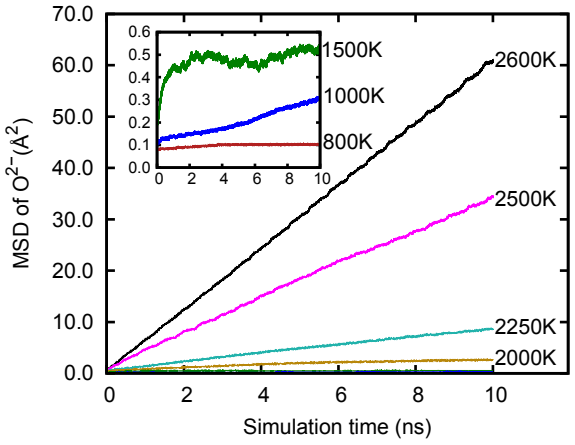
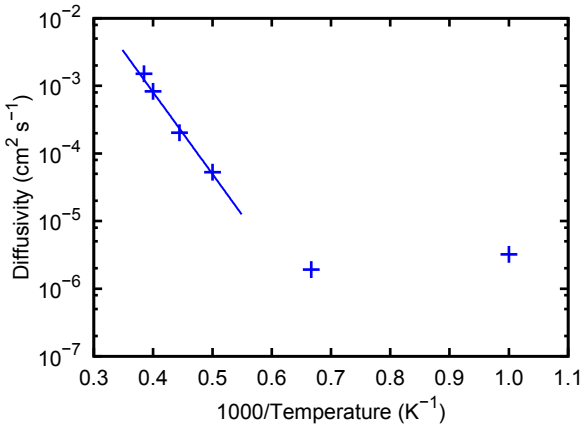


Figure 4: (a) An isosurface plot showing regions of low charge densities (dark-shaded) in the quasi-cubic structure with SrO interfaces. The two largest regions are labelled A and B respectively. (b) The trajectories of the O^{2-} ions projected onto the $x - z$ plane at 2250 K, aligned with the lattice in (a). (c) Illustration of the rotation of three O^{2-} ions, O1, O2 and O3, about a Zr^{4+} ion. (d) Illustration of the path of O^{2-} ions O3, O4 and O5 which contribute to long-range diffusion in the structure. Figure 6 shows (c) and (d) in more detail. The YSZ layer is defined as shown between figures (c) and (d).



(a)



(b)

Figure 5: (a) The MSD with time of O^{2-} ions within the YSZ layer in the configuration with SrO interfaces for simulated temperatures of 800 K - 2600 K, with the YSZ layer now defined as labelled in the Figure 4. Inset: magnification of the MSD for temperatures of 1500 K and below. (b) Arrhenius plot for O^{2-} ions within the YSZ layer in the configuration with SrO interfaces. For the calculation of activation energy, we consider only data obtained at 2000 K and above—the data points through which the line is drawn.

.

the YSZ layer to include the Y^{3+} ions as indicated in Figure 4. We therefore present results of the MSD of the O^{2-} ions within the YSZ layer only.

The variation of the O^{2-} ion MSD with time shown in Figure 5(a) indicates that there is no significant diffusion of the O^{2-} ions within 10 ns when the temperature is below 1000 K. We observe upon closer inspection (not shown here) of the O^{2-} ions displacements particularly between 1000 K to 2000 K that there are at times abrupt increases in the displacements. Analysis of the motion of the anions reveals that each of these increases corresponds not to a hopping of a single O^{2-} ion, but to a concerted motion of three O^{2-} ions. Figures 4(c), and 6 with clearer detail, illustrate this movement at 2000 K at 471.6 ps. The three ions involved are bonded to a common Zr^{4+} ion within the YSZ layer; this Zr^{4+} ion has sevenfold coordination with O^{2-} ions, with three O^{2-} ions to the right of the $x-y$ plane on which the Zr^{4+} ion lie. These three ions, labelled O1, O2 and O3 in the diagram, rotate about the Zr^{4+} ion

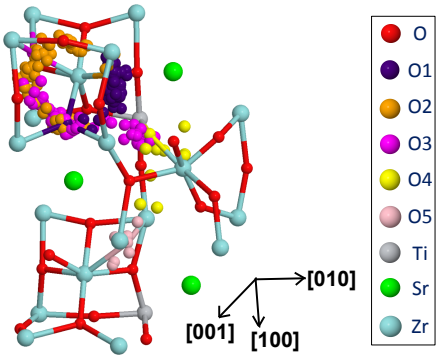


Figure 6: A series of snapshots showing the diffusion path of O^{2-} ions within the quasi-cubic YSZ layer of the structure with SrO interfaces. The rotation of O1, O2 and O3 ions in this instance is counter-clockwise.

.

roughly within a plane parallel to interfacial plane through about a third of a revolution. Only one such movement of the triple ions is observed at 1000 K throughout the simulated 2000 ps, corresponding to the small jump in the O^{2-} ion MSD and the subsequent plateau. At temperatures greater than 1000 K, more than one set of the triple ions participate in the rotation, some of which may rotate through several thirds of a revolution with frequency increasing with temperature. However, we note that this rotational movement does not contribute to long-range diffusion.

An additional second type of movement, a crossing of an O^{2-} ion to a neighbouring Zr^{4+} ion, is observed at temperatures of 2000 K and above. This is illustrated in Figure 4(d) at 2000 K after 490 ps. The O^{2-} ion O3, having rotated about its Zr^{4+} ion earlier, breaks its bond with the Zr^{4+} ion and travels approximately in the [010] direction to a neighbouring Zr^{4+} ion, forming a bond with the latter. This precipitates a third type of movement in which O^{2-} ion O4—whose lattice site is now the destination site of the ion O3—is being nudged away just as ion O3 begins its journey. Ion O4 travels down the path depicted with more detail in Figure 6, dipping underneath the latter Zr^{4+} ion. As it arrives at its destination, O^{2-} ion O5 currently bonded to this Zr^{4+} ion, is displaced away towards another Zr^{4+} ion in the $[1\bar{1}0]$ direction, as it would have been too close to the newly arrived ion O4. The perturbation of ion O5 initiates a triple ion rotation about its new Zr^{4+} ion, though this does not occur till later, at 620 ps. Contrary to the first type of movement, this second type clearly contributes to long-range diffusion of the anions.

The diffusion mechanism that we observe resembles the cooperative motion reported for Li^+ ions in $LiMgSO_4F$ [42], or that for O^{2-} ions in $La_{1-x}Ba_{1+x}GaO_{4-x/2}$[43]. It is worth noting that the pathways, predicted from classical MD simulations, cross through the regions identified to have low charge densities, calculated using DFT. The rotation of ions O1, O2 and O3 occurs within region A, while O^{2-} ion O4 passes through region B, labelled in Figure 4(a). Figure 4(b) shows the trajectories of the O^{2-} ions in the structure projected onto the $x-z$ plane, indicating that the paths are mostly parallel to the interface plane and confined within the YSZ layer. O^{2-} ions within the YSZ layer other than the five that we

have identified may also have been substantially displaced from their initial sites in the simulations with paths perpendicular to the interfacial plane; but their contribution to the calculated MSD is relatively smaller.

We extract the values of the diffusivities D of the O^{2-} ions at each temperature from the MSD plots using the Einstein relation:

$$\langle r^2 \rangle = 4D(t - t_0) + c \tag{4}$$

where $\langle r^2 \rangle$ is the MSD of the O^{2-} ions at time t from their initial positions at time t_0, and c is an arbitrary constant. The diffusion of the O^{2-} ions in the system is mainly 2-dimensional, hence the factor of 4. The values of D were then used to obtain the activation energy and pre-exponential factor D_0 by fitting the Arrhenius equation:

$$D = D_0 \exp\left(-\frac{E}{kT}\right). \tag{5}$$

where E is the activation energy for the O^{2-} ion diffusion, k is the Boltzmann constant, T is the temperature and D_0 is the pre-exponential factor.

In calculating the activation energy, we obtain different results depending on the temperature range as well as the range of O^{2-} ions that we select for the calculation of MSD. Figure 5(b) shows the Arrhenius plot for O^{2-} ions within the YSZ layer defined in Figure 4. If we consider all data points on the plot for temperatures between 1000 K - 2600 K, we would obtain an activation energy of about 0.80 eV. However, we observe that the data points do not fall neatly on a straight line. In fact, the data could be separated into two regimes: a low temperature regime below 2000 K and a high temperature regime above 2000 K. The reason for this is clear when we consider the diffusion mechanism that is activated in these two regimes. Below 2000 K, the motion of the O^{2-} ions is only rotational over the simulation time and so does not involve long range diffusion; above this temperature, there is long-range diffusion with breaking and forming of bonds. The Einstein relation is only valid when long-range diffusion is achieved in the system; we therefore neglect data for temperatures below 2000 K in our calculation for activation energy and only consider the steady-state regime.

The activation energy of the diffusion of O^{2-} ions in the YSZ layer is calculated to be 2.4 eV, with a preexponential factor of 0.0061 cm^2s^{-1}. Both these values are much higher than those reported for bulk YSZ with similar Y_2O_3 concentration using the same set of interatomic potentials [21, 44, 45], which are 0.7 eV and 8×10^{-5} cm^2s^{-1} respectively. Our calculated atypical values of activation energy and pre-exponential factor for diffusion are evidence of the unconventional diffusion mechanism, suggesting that the energy barrier for concerted motion of several ions, with only a little extra vacant space to facilitate it, is greater than the hopping of a single ion at a time to a vacancy similar in size to the ion.

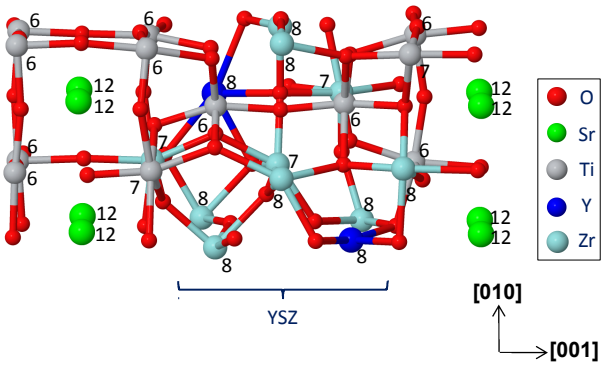


Figure 7: The coordination numbers of the cations with O^{2-} ions in the quasi-cubic YSZ/STO configuration with TiO_2 interfaces.

Furthermore, the stable structure of the ultrathin coherent YSZ on STO multilayer with SrO interfaces that we predict is a poor oxide ion conductor. This is in disagreement with the published experimental result by Garcia-Barriocanal *et al.* [12]; they reported an activation energy of 0.6 eV for the conductivity in a STO/$YSZ_{(1nm)}$/STO trilayer, which is significantly lower than that of typical bulk YSZ of ∼1.1 eV measured in experiments.

3.3. The quasi-cubic YSZ/STO structure with TiO_2 interfaces and its oxygen ion diffusivity

In our search for low energy YSZ/STO configurations in which the STO layers are terminated with TiO_2 planes, we did not obtain configurations with Sr^{2+}/Y^{3+} ions intermixing between the quasi-cubic YSZ and STO layers as we have found for configurations with SrO interfaces. We find that in this case, Sr^{2+}/Y^{3+} ion exchange between the layers is energetically unfavourable when the energies of the structures are evaluated using classical interatomic potentials, and observe the same trend when recalculating the energies within DFT. There was, nonetheless, intermixing of Ti^{4+}/Zr^{4+} ions between the layers which yields slightly more energetically favourable configurations in comparison to the phase-separated ones for many of the lower energy configurations obtained from our genetic algorithm simulations. Figure 1(b)(ii) shows the most stable configuration with TiO_2 interfaces that we have found, with the YSZ layer indicated in Figure 7. The diffused Ti^{4+} ions in the YSZ layer are within the same (001) atomic planes as the Y^{3+} ions in Zr^{4+} lattice sites, while these Zr^{4+} ions replace the TiO_2 ions at interfacial planes. Computing the energy difference between this configuration and its phase-separated counterpart, the energy of the former is lowered by 0.0961 eV per supercell.

As before, we compare the local coordination of the cations in this configuration to those in the bulk materials. The coordinations of the Zr^{4+} ions with O^{2-} ions range from sevenfold to eightfold (Figure 7), similar to those in the quasi-cubic structure with SrO interfaces but without any Zr^{4+} ions with sixfold coordination. Within the STO layer the coordinations of the Sr^{2+} and the Ti^{4+} ions are the expected twelvefold and sixfold respectively, though some of the Ti^{4+} ions at the interface planes as well as those within the YSZ layer are in sevenfold coordination. The Y^{3+} ions, being within the YSZ

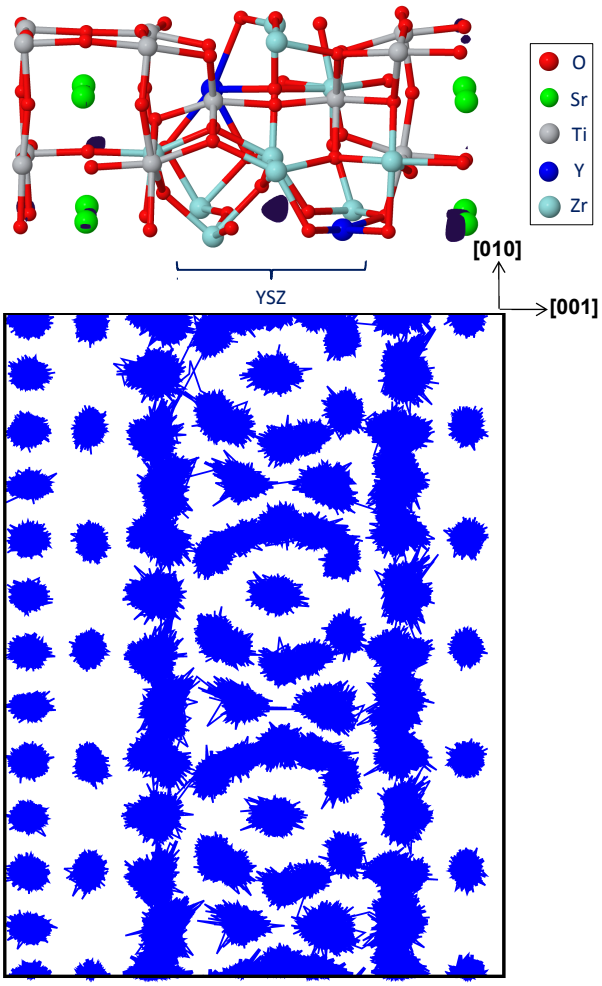


Figure 8: (Top) Regions of low charge density, dark-shaded, in the quasi-cubic multilayer with TiO_2 interfaces. (Bottom) The trajectory of the O^{2-} ions in this configuration, aligned with the lattice shown above.

layer, are eightfold-coordinated with O^{2-} ions as they would have been in bulk YSZ [46]. Thus the local coordinations of the cations in the YSZ layer is as varied as those in the YSZ/STO structure with SrO interfaces, and could not be identified as fluorite or other known oxides.

Unlike the configuration with SrO interfaces discussed in the previous section, we do not find any substantial region of low charge density in the YSZ/STO configuration with TiO_2 interfaces (Figure 8). The lack of well-defined vacancies must adversely affect the diffusivity of O^{2-} ions; from our MD simulations of the structure, we do not observe long range O^{2-} ion diffusion. We only observe some cooperative motion of the oxygen ions from 1750 K up to 2250 K both along and perpendicular to the interface, as indicated in Figure 8, but with limited displacement of the anions (Figure 9). Above this temperature range, the lattice becomes disordered and melts. In the absence of long range diffusion, we cannot extract meaningful diffusivities and hence are unable to calculate the activation energy for O^{2-} ion motion in this configuration. Nevertheless, it is clear that the diffusivity of O^{2-} ions in our predicted YSZ/STO multilayered structure with TiO_2 interfaces is lower than that with SrO interfaces, with the latter already showing reduced diffusivity compared to YSZ in the bulk.

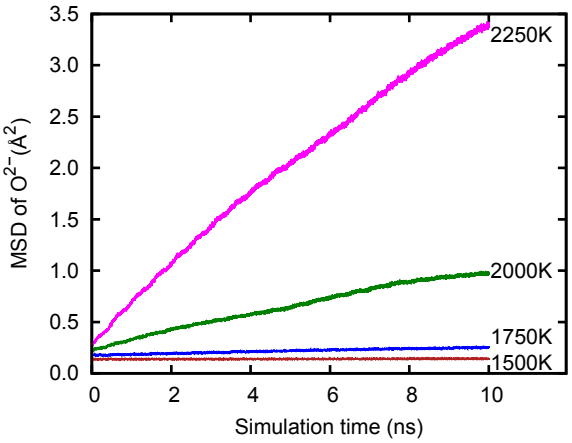


Figure 9: The MSD of the O^{2-} ions within the YSZ layer for temperature between 1500 K and 2250 K.

Our diffusivity results for both YSZ/STO systems with SrO and TiO_2 interfaces are clearly not in agreement with experimental values [12]. Although we have conducted an extensive structure search on the YSZ/STO interface, we cannot discount the possibility that the most stable one found by our search method is not indeed the global minimum. On the other hand, metastable phases can be fabricated depending on experimental conditions. Nevertheless, at the time of writing, experimental evidence[47] for the structure of the YSZ layer is consistent with one of a substituted perovskite, not unlike the type we have discovered here and called 'quasi-cubic'. The experimental evidence indicates that the perovskite STO layers extend into the YSZ region, retaining the perovskite lattice even within the YSZ region, with Zr^{4+} substituting onto the Ti^{4+} sites. From observing a small decrease in the concentration Sr^{2+} within this region, the authors infer a substitution of Y^{3+} onto the Sr^{2+} sites. They also find that the STO layers are Ti^{4+}-deficient, supporting our result for the quasi-cubic structure with SrO interfaces being the most stable across almost the whole range of possible μ_{TiO_2}.

Since Garcia-Barriocanal *et al.* observed an ordered interface structure at least as far as the cation sublattice is concerned[12], we have assumed in our work an interface that is crystalline and stoichiometric. Our assumption of perfect stoichiometry in the YSZ layer may or may not be the case in reality; non-stoichiometry would affect the interface structure and thus modify the anion diffusivity. Yet, as aforementioned, some have suggested that the conductivity measured in the YSZ/STO layers by Garcia-Barriocanal *et al.* have electronic rather than ionic character[13, 14, 15, 16, 20]. One may calculate the electronic properties of the structures that we have predicted in this work to determine the electronic conductivity, using more accurate functionals, but such calculations are beyond the scope of the present work.

4. Conclusions

We have considered several interface structures of YSZ/STO multilayered system with different termination planes of the STO layer, derived by exploring the space of structures with a genetic algorithm in which the energies are evaluated with classical interatomic potentials. Refining their energies and structures with DFT-based calculations, we find a structure of the YSZ layer that is different from those of common oxides, and referred to here as 'quasi-cubic'. The cation sublattice of this structure resembles that of perovskite as well as fluorite, though the local coordinations of some cations with the anions differ from those in either lattice. Configurations with intermixing between the YSZ and STO layers are energetically more favourable than those with abrupt interfaces between the layers.

Calculations of O^{2-} ion diffusivities for the predicted structures do not agree with reported experimental values for STO/YSZ multilayers. For the configuration with SrO termination planes, we find that there are several small pockets of low electron density rather than the expected single localised region. The diffusion mechanism is therefore unlike the conventional vacancy hopping mechanism expected in bulk YSZ. In fact, we show that there are two regimes of cooperative O^{2-} ion diffusion in such configurations: a rotational one occurring at lower temperatures and an additional displacive one at higher temperatures. Only the latter contribute to long-range diffusion from which we calculate an activation energy and pre-exponential factor much higher than that in bulk YSZ, evidence of the unconventional diffusion mechanism. In the calculation of the activation energy, we demonstrate the need to exclude data from the lower temperature range in which only local, rotational motion of the anions occurs. The inclusion of such data would have reduced the calculated activation energy by about two-thirds, i.e. to a value lower than that in bulk YSZ, and thereby changed our conclusion.

We also examine the configuration with the TiO_2-terminated STO layer which is only stable at high μ_{TiO_2} within a limited range. The lack of vacancies in this configuration limits the diffusivity of the O^{2-} ions; in fact we do not observe any long-range diffusion of the anions and thus could not calculate an activation energy. We therefore conclude that our predicted coherent YSZ/STO structure, whether the STO layer is terminated by SrO or TiO_2 planes, exhibits a suppression of ionic conductivity.

Acknowledgements

The calculations were performed on the Imperial College High Performance Computing facilities as well as HECToR, the UK's national high-performance computing service, which is provided by UoE HPCx Ltd at the University of Edinburgh, Cray Inc and NAG Ltd, and funded by the Office of Science and Technology through EPSRC's High End Computing Programme (EP/L000202). The authors acknowledge support of the Thomas Young Centre under grant TYC101.

References

[1] C. J. Howard, R. J. Hill, B. E. Reichert, Structures of ZrO_2 polymorphs at room temperature by high-resolution neutron powder diffraction, Acta Crystallographica Section B 44 (1988) 116–120.

[2] S. Fabris, A. T. Paxton, M. W. Finnis, A stabilization mechanism of zirconia based on oxygen vacancies only, Acta Materialia 50 (2002) 5171–5178.

[3] L. Malavasi, C. A. J. Fisher, M. S. Islam, Oxide-ion and proton conducting electrolyte materials for clean energy applications: structural and mechanistic features, Chemical Society Reviews 39 (2010) 4370–4387.

[4] J. A. Kilner, M. Burriel, Materials for intermediate-temperature solid-oxide fuel cells, Annual Review of Materials Research 44 (2014) 365–393.

[5] B. Steele, A. Heinzel, Materials for fuel-cell technologies, Nature 414 (2001) 345–352.

[6] B. Yildiz, stretching the energy landscape of oxideseffects on electrocatalysis and diffusion, Mrs Bulletin 39 (2014) 147–156.

[7] C. Korte, J. Keppner, A. Peters, N. Schichtel, H. Aydin, J. Janek, Coherency strain and its effect on ionic conductivity and diffusion in solid electrolytesan improved model for nanocrystalline thin films and a review of experimental data, Physical Chemistry Chemical Physics 16 (2014) 24575–24591.

[8] J. A. Hirschfeld, H. Lustfeld, First-principles study and modeling of strain-dependent ionic migration in zro_2, Physical Review B 84 (2011) 224308.

[9] C. Korte, N. Schichtel, D. Hesse, J. Janek, Influence of interface structure on mass transport in phase boundaries between different ionic materials, Monatshefte für Chemie / Chemical Monthly 140 (2009) 1069–1080.

[10] I. Kosacki, C. M. Rouleau, P. F. Becher, J. Bentley, D. H. Lowndes, Nanoscale effects on the ionic conductivity in highly textured YSZ thin films, Solid State Ionics 176 (2005) 1319–1326.

[11] B. Li, J. Zhang, T. Kaspar, V. Shutthanandan, R. C. Ewing, J. Lian, Multilayered YSZ/GZO films with greatly enhanced ionic conduction for low temperature solid oxide fuel cells, Physical Chemistry Chemical Physics 15 (2013) 1296–1301.

[12] J. Garcia-Barriocanal, A. Rivera-Calzada, M. Varela, Z. Sefrioui, E. Iborra, C. Leon, S. J. Pennycook, J. Santamaria, Colossal ionic conductivity at interfaces of epitaxial ZrO_2:Y_2O_3/$SrTiO_3$ heterostructures, Science 321 (2008) 676–680.

[13] X. Guo, Comment on "Colossal ionic conductivity at interfaces of epitaxial ZrO_2:Y_2O_3/$SrTiO_3$ heterostructures", Science 324 (2009) 465.

[14] X. Guo, J. Maier, Ionically conducting two-dimensional heterostructures, Advanced Materials 21 (2009) 2619–2631.

[15] N. Schichtel, C. Korte, D. Hesse, J. Janek, Elastic strain at interfaces and its influence on ionic conductivity in nanoscaled solid electrolyte thin films — theoretical considerations and experimental studies, Phys Chem Chem Phys 11 (2009) 3043–8.

[16] M. Gerstl, G. Friedbacher, F. Kubel, H. Hutter, J. Fleig, The relevance of interfaces for oxide ion transport in yttria stabilized zirconia (YSZ) thin films, Physical Chemistry Chemical Physics 15 (2013) 1097–1107.

[17] K. Otsuka, A. Kuwabara, A. Nakamura, T. Yamamoto, K. Matsunaga, Y. Ikuhara, Dislocation-enhanced ionic conductivity of yttria-stabilized zirconia, Applied Physics Letters 82 (2003) 877–879.

[18] A. Cavallaro, B. Ballesteros, R. Bachelet, J. Santiso, Heteroepitaxial orientation control of YSZ thin films by selective growth on SrO-, TiO_2-terminated $SrTiO_3$ crystal surfaces, CrystEngComm 13 (2011) 1625–1631.

[19] A. Rivera-Calzada, M. R. Diaz-Guillen, O. J. Dura, G. Sanchez-Santolino, T. J. Pennycook, R. Schmidt, F. Y. Bruno, J. Garcia-Barriocanal, Z. Sefrioui, N. M. Nemes, M. Garcia-Hernandez, M. Varela, C. Leon, S. T. Pantelides, S. J. Pennycook, J. Santamaria, Tailoring interface structure in highly strained YSZ/$SrTiO_3$ heterostructures, Advanced Materials 23 (2011) 5268–5274.

[20] A. Cavallaro, M. Burriel, J. Roqueta, A. Apostolidis, A. Bernardi, A. Tarancón, R. Srinivasan, S. N. Cook, H. L. Fraser, J. A. Kilner, D. W. McComb, J. Santiso, Electronic nature of the enhanced conductivity in YSZ–$SrTiO_3$ multilayers deposited by PLD, Solid State Ionics 181 (2010) 592–601.

[21] G. Dezanneau, J. Hermet, B. Dupé, Effects of biaxial strain on bulk 8% yttria-stabilised zirconia ion conduction through molecular dynamics, International Journal of Hydrogen Energy 37 (2012) 8081–8086.

[22] A. Kushima, B. Yildiz, Oxygen ion diffusivity in strained yttria stabilized zirconia: where is the fastest strain?, Journal of Materials Chemistry 20 (2010) 4809–4819.

[23] X.-M. Bai, Y. Zhang, M. R. Tonks, Strain effects on oxygen transport in tetragonal zirconium dioxide, Physical Chemistry Chemical Physics 15 (2013) 19438–19449.

[24] F. Li, R. Lu, H. Wu, E. Kan, C. Xiao, K. Deng, D. E. Ellis, The strain effect on colossal oxygen ionic conductivity in nanoscale zirconia electrolytes: a first-principles-based study, Physical Chemistry Chemical Physics 15 (2013) 2692–2697.

[25] W. Araki, Y. Arai, Optimum strain state for oxygen diffusion in yttria-stabilised zirconia, Solid State Ionics 190 (2011) 75–81.

[26] D. S. Aidhy, B. Liu, Y. Zhang, W. J. Weber, Strain-induced phase and oxygen-vacancy stability in ionic interfaces from first-principles calculations, The Journal of Physical Chemistry C 118 (2014) 30139–30144.

[27] W. Cheah, M. W. Finnis, Structure of multilayer $ZrO_2/SrTiO_3$, Journal of Materials Science 47 (2012) 1631–1640.

[28] T. J. Pennycook, M. J. Beck, K. Varga, M. Varela, S. J. Pennycook, S. T. Pantelides, Origin of colossal ionic conductivity in oxide multilayers: Interface induced sublattice disorder, Physical Review Letters 104 (2010) 115901.

[29] T. J. Pennycook, M. P. Oxley, J. Garcia-Barriocanal, F. Y. Bruno, C. Leon, J. Santamaria, S. T. Pantelides, M. Varela, S. J. Pennycook, Seeing oxygen disorder in $YSZ/SrTiO_3$ colossal ionic conductor heterostructures using EELS, The European Physical Journal - Applied Physics 54 (2011) 33507.

[30] A. L. S. Chua, N. A. Benedek, L. Chen, M. W. Finnis, A. P. Sutton, A genetic algorithm for predicting the structures of interfaces in multicomponent systems, Nature Materials 9 (2010) 418–422.

[31] N. A. Benedek, A. L. S. Chua, C. Elsasser, A. P. Sutton, M. W. Finnis, Interatomic potentials for strontium titanate: An assessment of their transferability and comparison with density functional theory, Physical Review B (Condensed Matter and Materials Physics) 78 (2008) 064110.

[32] M. A. McCoy, R. W. Grimes, W. E. Lee, Phase stability and interfacial structures in the $SrO–SrTiO_3$ system, Philosophical Magazine A 75 (1997) 833 – 846.

[33] M. O. Zacate, L. Minervini, D. J. Bradfield, R. W. Grimes, K. E. Sickafus, Defect cluster formation in M_2O_3-doped cubic ZrO_2, Solid State Ionics 128 (2000) 243–254.

[34] S. J. Clark, M. D. Segall, C. J. Pickard, P. J. Hasnip, M. J. Probert, K. Refson, M. C. Payne, First principles methods using CASTEP, Zeitschrift für Kristallographie 220 (2005) 567–570.

[35] C. G. Broyden, The convergence of a class of double-rank minimization algorithms, IMA Journal of Applied Mathematics 6 (1970) 222–231.

[36] R. Fletcher, A new approach to variable metric algorithms, The Computer Journal 13 (1970) 317–322.

[37] D. Goldfarb, A family of variable metric methods derived by variational means, Mathematics of Computation 24 (1970) 23–26.

[38] D. Shanno, Conditioning of quasi-Newton methods for function minimization, Mathematics of Computation 24 (1970) 647–656.

[39] J. D. Gale, A. L. Rohl, The general utility lattice program (GULP), Molecular Simulation 29 (2003) 291–341.

[40] Y. Y. Zhang, R. Mishra, T. J. Pennycook, A. Y. Borisevich, S. J. Pennycook, S. T. Pantelides, Oxygen disorder, a way to accommodate large epitaxial strains in oxides, Advanced Materials Interfaces (2015).

[41] L. Pauling, The principles determining the structure of complex ionic crystals, Journal of the American Chemical Society 51 (1929) 1010–1026.

[42] M. Salanne, D. Marrocchelli, G. W. Watson, Cooperative mechanism for the diffusion of Li^+ ions in $LiMgSO_4F$, The Journal of Physical Chemistry C 116 (2012) 18618–18625.

[43] E. Kendrick, J. Kendrick, K. S. Knight, M. S. Islam, P. R. Slater, Cooperative mechanisms of fast-ion conduction in gallium-based oxides with tetrahedral moieties, Nature materials 6 (2007) 871–875.

[44] R. L. González-Romero, J. J. Meléndez, D. Gómez-García, F. L. Cumbrera, A. Domínguez-Rodríguez, A molecular dynamics study of grain boundaries in YSZ: Structure, energetics and diffusion of oxygen, Solid State Ionics 219 (2012) 1–10.

[45] A. Tarancón, A. Morata, F. Peiró, G. Dezanneau, A molecular dynamics study on the oxygen diffusion in doped fluorites: The effect of the dopant distribution, Fuel Cells 11 (2011) 26–37.

[46] A. Bogicevic, C. Wolverton, G. M. Crosbie, E. B. Stechel, Defect ordering in aliovalently doped cubic zirconia from first principles, Physical Review B 64 (2001) 014106.

[47] D. W. McComb, Manuscript in preparation.